Geometrical Based Method for the Uncertainty Quantification of Correlated Aircraft Loads

Irene Tartaruga[1]
Jonathan E. Cooper[2]
Pia Sartor[3]
Mark H. Lowenberg[4]
Yves Lemmens[5]

Abstract

The identification of the critical load cases, aircraft configuration and flight conditions is a vital step in the aircraft design process; in particular the loads correlated at individual measurement stations, and between different stations, are of great interest. Typically, the correlation of various 'Interesting Quantities', such as bending moment and torque, is described using the so called 'potato plot', which is obtained by plotting Interesting Quantities time histories against each others. It is of interest to predict the effects of uncertainty in the structural and aerodynamic parameters on the correlated quantities in an efficient way. A geometrically based method is described enabling identification of probabilistic bounds for the correlated loads whilst still capturing all the information related to the critical cases. The method is demonstrated using gust loads acting on a representative civil jet aeroelastic numerical model, and very accurate yet efficient results are found in comparison to a Monte Carlo Simulation.

1 Introduction

A key part of the aircraft design process is the identification of the critical loads which can be used to determine maximum stress levels, and hence structural sizing, across the structure [23]. A wide range of load cases must be considered, including gusts, flight manoeuvres, landings, braking and taxiing, etc, as the critical cases are not known a-priori. Therefore, simulated loads cases are applied to detailed aeroelastic models [5][13] [23] in order to determine the critical cases and the corresponding aircraft configuration and flight conditions for a range of different Interesting Quantities (IQs), e.g. bending moments, shear forces and torque. The certification of large commercial aircraft is defined by the EASA CS-25 (Certification Specifications) or FAR-25 airworthiness regulations to assure structural integrity over the operating environment of the aircraft; they also define the range of load cases that has to be accounted for and the structural design is based upon the worst load cases. Typically, several thousand values of IQs must be considered, and a simplistic estimate of the number of analyses required to cover all possible conditions (e.g. mass distribution, control laws, flight condition, gust gradient, etc.) gives 10 million [11]. Even with simplistic aircraft models being used, this is an infeasible number of separate simulations [11]. Furthermore, these analyses have to be repeated (known as a loads cycle) every time that there is an update in the aircraft structure [8], and within the modern civil aircraft industry each of these loads cycles takes a considerable time. Aircraft loads are a 'living' database which is regularly updated during the course of the whole aircraft life.

The importance in considering the presence of uncertainty in loads computations has recently become recognised, and it significantly increases the number of required analyses. However, most work in uncertainty analysis applied to aeroelastic systems has concentrated upon the effect of uncertainties on critical phenomena such as flutter and divergence [4] [14] [1] [15] [18] [17] rather than loads.

[1] [2] [3] [4] University of Bristol, Dept. of Aerospace Engineering
Queens Building, University Walk, Bristol, BS8 1TR, United Kingdom
[5] Siemens
Interleuvenlaan 68, 3001 Leuven, Belgium

Previous work in the FFAST FP7 project [11] [10] [8] [9] has investigated the use of several surrogate modeling and optimization methods for fast and efficient prediction of the worst case gust loads for each IQ independently. Figure 2 shows typical responses of wing root bending moment to different length '1 - Cosine' (1MC) vertical gusts. Previous work determined the largest maximum and minimum loads resulting from the gusts across the design and operating space. However, it is essential to take into account the effect of correlations between IQs (e.g. bending moment and torque) as the principal stresses depend upon 2D or even 3D loads. By plotting the time histories of each IQ against each other, as seen in Figure 3, the worst cases are defined by the outlying points of the correlated loads plot, known as a convex hull or 'potato plot'. A very preliminary investigation relating to the uncertainty quantification of correlated gust envelopes was undertaken [9] using a simple 2 DOF aeroelastic model and exploiting the Polynomial Chaos Expansion (PCE)[2] [24] [3].

An initial investigation related to the uncertainty quantification of correlated gust envelopes was undertaken by the authors [19] using a Singular Value Decomposition (SVD) based method combined with surrogate modelling techniques. This approach enables very efficient calculation of all the IQ time histories at any possible point in the design space without losing accuracy compared to Monte Carlo Simulations (MCS) [19] [21]. Two approaches were considered to propagate the uncertainty in the computations, namely an interval method and a probabilistic approach. These two approaches can be adopted to deal with uncertainty for each IQ independently. Regarding the uncertainty in terms of correlated loads, the interval approach can be adopted to exactly identify the extreme worst case scenario without paying attention to the actual probabilistic occurrence of the loads. The probabilistic approach presented in [19] is based on the use of quantiles in terms of time-history quantities and could lead to imprecise results.

In this work, a method is developed that enables a probabilistic uncertainty propagation of the quantile-outer bounds for the loads 'potato' plots and exact identification of quantile-bounds and the critical cases using a geometric approach. This geometrical based method exploits the previously developed SVD based method [19] and an investigation is also undertaken into the possible benefits of using the Higher Order Singular Value Decomposition (HOSVD) [6]. The developed method retrieves information for loads correlated in time and in space associated with a desired confidence level; it relates the identified critical cases back to the corresponding configurations (e.g. structural parameters), load cases/manoeuvres and flight conditions. The method has been validated and the accuracy demonstrated using a representative civil jet aeroelastic numerical model and comparing with results from a MCS. Variable length 1MC vertical gusts are considered as the load cases and the engine mass and pylon stiffness are allowed to vary. The worst case wing root bending moment and torque are determined under the presence of uncertainty on the structural parameters.

2   Motivation

During the design process and certification of an aircraft the analysis of a very large number (10 M) of load cases and configurations is required. The traditional load case derivation and analysis process requires a significant time cost. Also the accuracy of the results is not quantified in terms of the assumptions made to try to simplify the analysis and the presence of uncertainties in the system. To tackle these issues, the proposed method is developed in order to cope with the presence of uncertainties in the system while correctly identifying the probabilistic bounds for the loads 'potato' plots. Moreover, the process has been devised in order to reduce the number of load cases to be considered during the design process and certification. Once the uncertain bounds for the correlated aircraft loads are determined, the critical load cases can be identified and
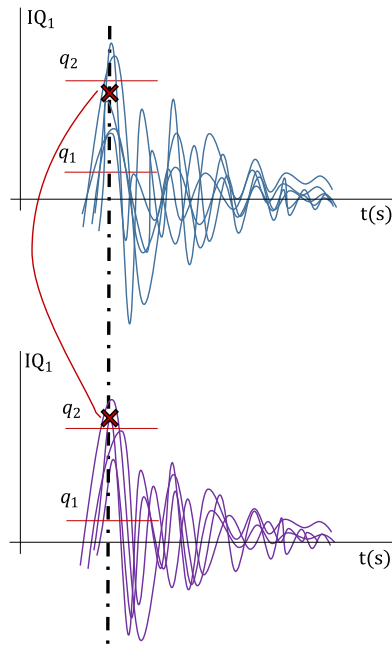
Figure 1: Example in which the assumption adopted in the quantile approach [19] can lead to imprecise results.

related back to the configuration, input loads/manoeuvres and flight condition. In a previous investigation by the authors to probabilistically describe the correlated loads [19], a quantile approach was developed. However, such an approach implies the assumption that all the correlated quantities are inside the quantile interval; in other words if one IQ has its value inside the defined quantile-interval then the same is assumed to happen for all the other IQs. However, this is not always the case, as Figure 1 shows, and this assumption can lead to errors in the prediction of the convex hull uncertainty bounds.

The developed geometrical based method does not rely on the above assumption and allows the quantile-outer bounds for the loads 'potato' plots to be correctly identified. It is also worth remarking that the method is totally general with no limit on the type of loads and IQs that are considered.

3 Modelling, Loads and Uncertainty Considerations

The numerical model used to demonstrate and validate the method is the FFAST model [11], a representative civil jet aeroelastic model whose nominal weights and main dimensions are reported in [19]. The structural model of the aircraft is a beam-stick representation with lumped masses (Figure 4) and the aerodynamics was modelled using the Doublet-Lattice Method (DLM).

1MC vertical gusts were applied to the model using gust lengths defined in the airworthiness regulations [23]. Figures 2 and 3 show examples of an IQ time history and a typical correlated load 'potato plot' obtained in response to 1MC gusts for different gust lengths (L_g). The resulting bending moment and torque time histories from the gust loads at 10 different wing stations were considered for the validation.

Uncertainty is introduced through some of the structural parameters, namely the mass of engine and the pylon stiffness (Young's Modulus). These have been probabilistically modelled assuming Gaussian PDFs as shown in Table 1. The statistical variation of the pylon Young Modulus and the mass of engine are taken from results presented in [2] and [22], respectively.

Table 1: Description adopted for the uncertain parameters.

	Mean μ	COV	Standard Deviation	Variation
Mass of Engine	8694.93 kg	0.039	339.1 kg	$\pm 10\%$
Pylon Young Modulus	$69 \cdot 10^9$ Pa	0.1	$69 \cdot 10^8$ Pa	$\pm 20\%$

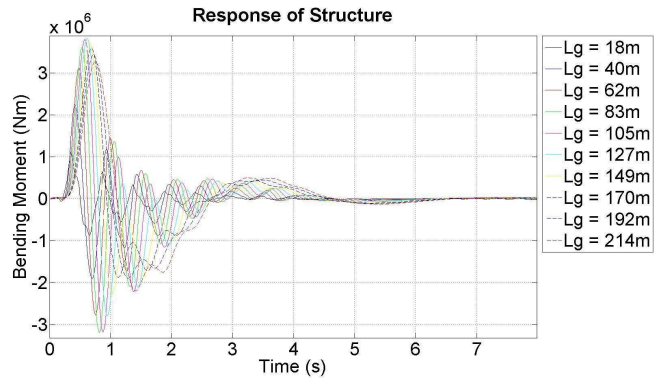
Figure 2: Time Histories of Bending Moment for Different Gust Lengths.

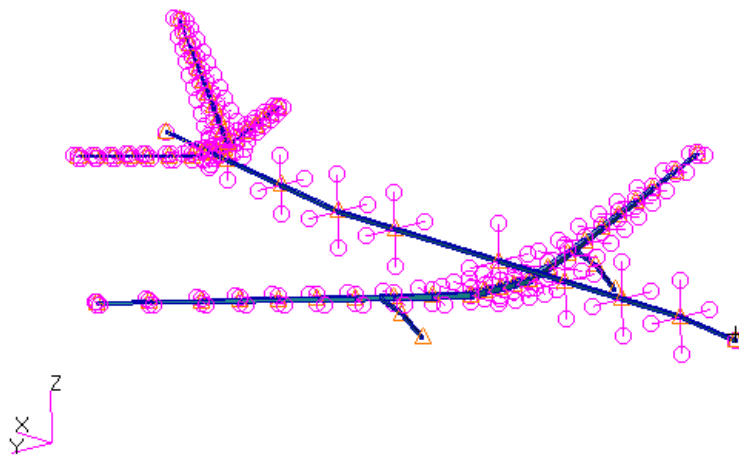**Figure 3:** 'Potato Plot' description of Correlated Loads for Different Gust Lengths.
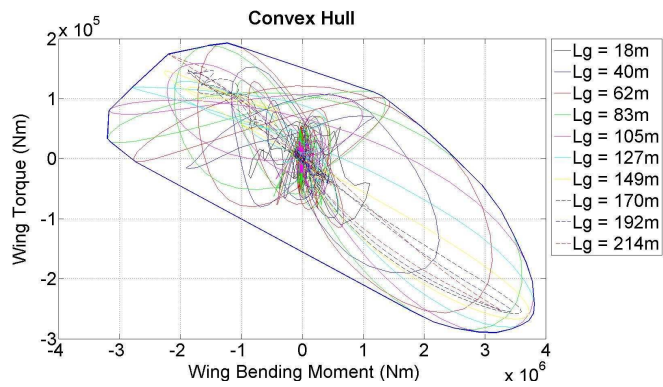
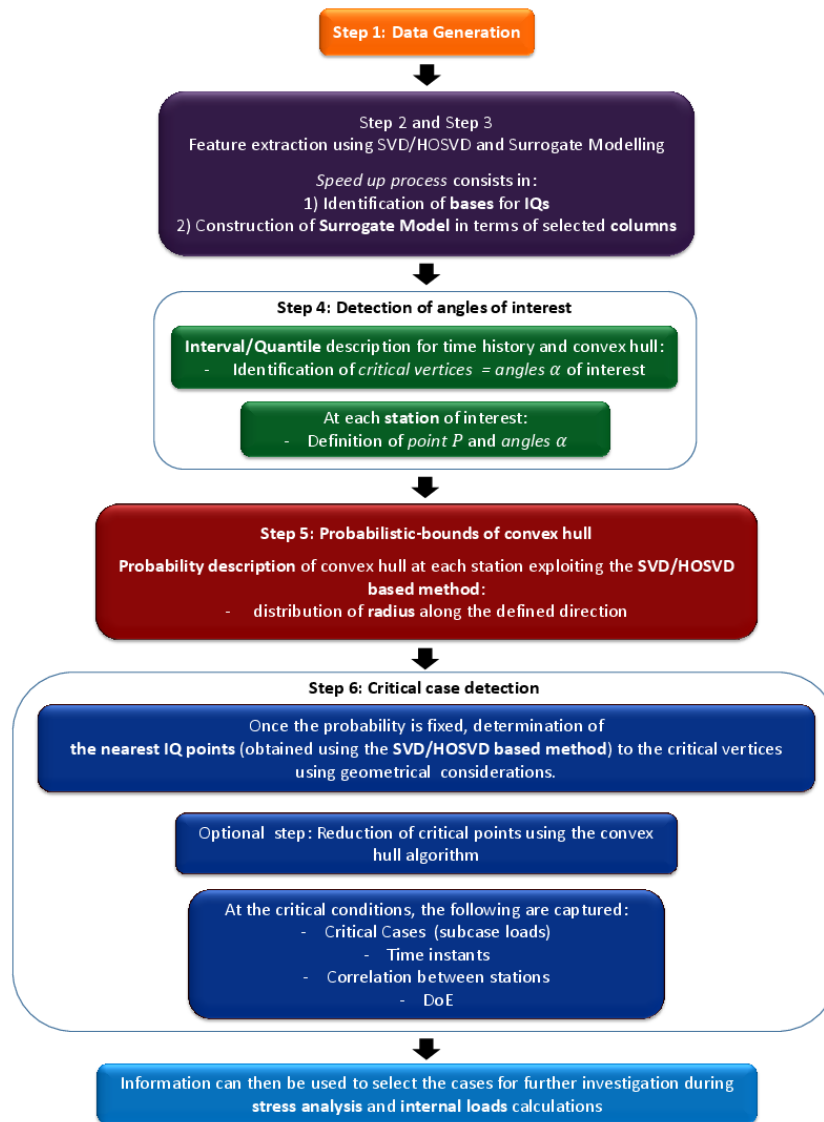**Figure 4:** Structural model of the aircraft.

**Figure 5:** Flow chart of the Geometrical Based Method.

4   Geometrical Based Method

A Geometrical method has been developed to predict the effect of uncertainties on correlated aircraft loads and was implemented using MATLAB . It consists of six steps which are shown in Figure 5. Initially, numerical simulations are performed (step 1) at various points in the parameter space (e.g. gust length, engine mass, pylon stiffness) in order to train the reduced order SVD/HOSVD surrogate models (steps 2 and 3). The apexes of the convex hull (potato plots) are then found relating to a central point and radii (step 4) from which the effect of uncertainty along each radius is determined (step 5). Finally, the geometric information generated from the previous step is transformed to define the critical correlated loads and corresponding case information (step 6). In the following sections each step of interest is described in detail.

Step 1: Data generation

Initially, the sampling plane to be considered for the generation of IQs, is defined. A suitable sampling method (e.g. Latin Hypercube Sampling, Hamilton or Sobol sequences) is selected and IQs are determined for three types of sampling points, using the numerical model that best represents the analysed problem. These sampling points are:

Figure 6: Data matrix adopted to apply the SVD for the ith interesting quantity or 'slice' of the data tensor in the 2D dimension $(1, i^{th})$ used to apply the HOSVD.
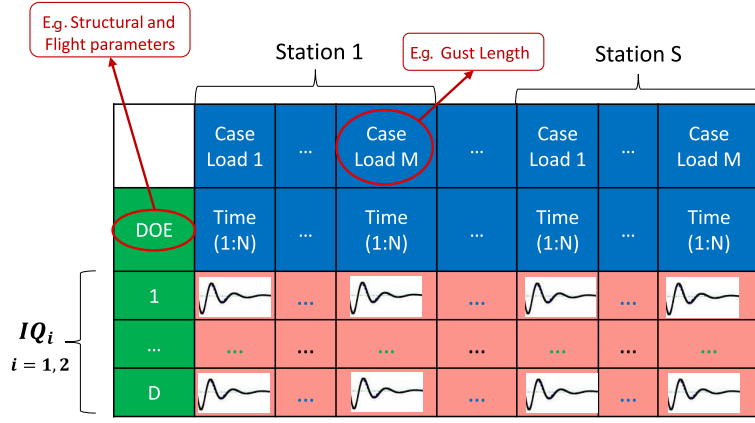
1. training points, which are used to train surrogate models adopted to speed up the Uncertainty Quantification (UQ)

2. validation points for the surrogate models, which are needed to validate the trained surrogate models

3. validation points for the results given by the UQ, which are used to obtain an 'actual' but time consuming UQ. The 'actual' UQ is performed using Monte Carlo Simulations analysis. There would be no benefit in performing this last step in practice due to computational limitations and it would also negate the reason for developing the methodologies.

Step 2: Feature Extraction using Singular Value Decomposition (SVD) / High Order Singular Value Decomposition (HOSVD)

Once the data of interest has been generated, a suitable data matrix or a tensor is constructed from the time histories related to the training points for each of the IQs or for all of the IQs, respectively. Then, the SVD [19] or HOSVD [20] can be applied for feature extraction. Figure 6 shows the data matrix or 'slice' of the data tensor in the 2D dimensions $(1, i^{th})$ adopted to deal with correlated time-histories of aircraft loads. Using the bending moment and the torque at the 10 stations along each wing that have been selected as IQs, the matrix defined for each IQ, or the 'slice' of the tensor constructed for all the IQs, has as many rows as the number of parameter variations (e.g. engine mass, pylon stiffness) (D) and as many columns as the product of the number of time steps in each response (N), the number of configurations/ environmental conditions (e.g. load cases as gust lengths, altitudes) (M) and the number of stations of interest (S). Thus, the dimensions of each matrix / 'slice' are $(D) \times (N \times M \times S)$. The total dimensions of the tensor are $(D) \times (N \times M \times S) \times 2$, the last dimension is equal to the number of analysed IQs that in the present problem are the bending moment and the torque. For the sake of clarity the tensor considered is shown in Figure 7, from which the 'slice' shown in Figure 6 can be taken for one of the IQs.

The SVD based method [19] performs a SVD on the data matrix $\mathbf{A}$ using the training data such that

$$\mathbf{A} = \mathbf{U}\boldsymbol{\Sigma}\mathbf{V^T} \tag{1}$$

The rank of the data matrix $\mathbf{A}$ (and so of the model order) is reduced by selecting the most significant singular values in $\boldsymbol{\Sigma}$. The product of the reduced 'singular values matrix' $\boldsymbol{\Sigma_k}$ and the transpose of the 'right singular
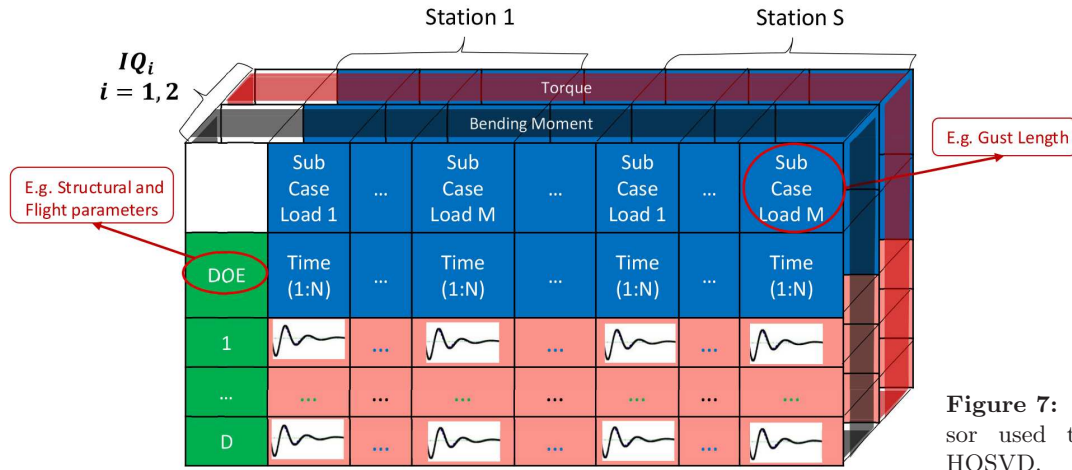
Figure 7: Data tensor used to apply the HOSVD.

vector matrix' $\mathbf{V_k^T}$ is adopted as basis and kept constant over the considered range of parameter variation. A surrogate model is then constructed for each column of the reduced 'left singular vector matrix' $\mathbf{U_k}$. The surrogates can then be used to perform the uncertainty quantification. For any desired set of parameter values, a time history can be reconstructed by multiplying the basis $\mathbf{\Sigma_k V_k^T}$ by the surrogates of $\mathbf{U_k}$ evaluated at the selected parameter values.

The HOSVD can be seen as a generalization of the SVD in higher dimension, so whereas the SVD is applied to matrices, the HOSVD is applied to tensors.

Given a tensor $\mathcal{A} \in \mathbb{R}^{I_1 \times I_2 ... \times I_D}$ the HOSVD can be expressed as [12] [6]:

$$\mathcal{A} = \mathcal{S} \times_1 \mathbf{U^1} \times_2 \mathbf{U^2} ... \times_D \mathbf{U^D} \qquad (2)$$

where

- the vector U_i^n is an ith n-mode singular vector; the superscript is adopted to refer to the particular number of the considered mode singular vector. There are as many mode singular vectors as the dimension of the tensor

- I_i is used as the general size of the dimension i, for instance I_1 is the dimension of the 1-mode singular vector $\mathbf{U^1}$

- the symbol $\times_i$ is adopted for the n-mode product. In general the n-mode product of a tensor $\mathcal{A} \in \mathbb{R}^{I_1 \times I_2 ... \times I_D}$ by a matrix $\mathbf{U} \in \mathbb{R}^{J \times I_n}$ is denoted by $\mathcal{A} \times_\mathbf{n} \mathbf{U}$ and is an $I_1 \times I_2 \times ... \times I_{n1} \times J \times I_{n+1} ... \times I_D$ tensor of which the entries are given by [12]

$$\mathcal{A} \times_\mathbf{n} \mathbf{U} = \sum_{\mathbf{i_n}} \mathbf{a_{i_1 i_2 ... i_{n1} i_{n_i} i_{n+1} ... i_N} u_{j i_n}} \qquad (3)$$

- $\mathcal{S}$ is the core tensor, whose dimension are $I_1 \times I_2 ... \times I_D$, dim $\mathbf{U^i} = I_i \times I_i$. Fixing the nth index to α the subtensors $\mathcal{S}_{\mathbf{i_n} = \alpha}$ is obtained, which have the properties of:

  i all-orthogonality: two subtensors $\mathcal{S}_{\mathbf{i_n} = \alpha}$ and $\mathcal{S}_{\mathbf{i_n} = \beta}$ are orthogonal for all possible values of n and for α and β subject to $\alpha \neq \beta$:

  $$\langle S_{i_n = \alpha}, S_{i_n = \beta} \rangle = 0 \qquad \text{when} \qquad \alpha = \beta, \qquad (4)$$

ii ordering

$$\|S_{i_{n=1}}\| \geq \|S_{i_{n=2}}\| \geq ... \geq \|S_{i_{n=I_n}}\| \geq 0 \qquad (5)$$

for all possible values of n.

$\|\|$ is the Frobenius-norm and $\|S_{i_{n=i}}\|$ is the ith of the n-mode singular values of $\mathcal{A}$, symbolized by σ_i^n .

As for the SVD, the HOSVD gives the possibility of reducing the dimensions of the problem by suitably decreasing the rank of the tensor. When a reduction is considered, one refers to the so called truncated SVD or multilinear singular value decomposition (mlsvd) for the SVD and HOSVD, respectively. The rank reduction in the HOSVD is done here by looking at the 'matrices unfolding' [12] [6], which is a matrix representation to which the HOSVD can be related. Given a tensor $\mathcal{A}$ there are as many matrices unfolding as the dimension of the tensor (here 3). The matrices unfolding are defined using the tensor dimensions in a cyclic way, in our case the dimensions are $I_1 = D, I_2 = (N \times M \times S), I_3 = 2$. The mathematical definition is [12]:

Assume an Nth order tensor $\mathcal{A} \in \mathbb{R}^{I_1 \times I_2 ... \times I_N}$. The matrix unfolding related to the nth dimension of the tensor (i.e. to the nth mode) $\mathbf{A_n} \in \mathbb{R}^{I_n \times (I_{n+1} I_{n+2} ... I_N I_1 I_2 ... I_{n1}}$ contains the element $a_{i_1 i_2 ... i_N}$ at the position with row number i_n and column number equal to $(i_{n+1}1)I_{n+2}I_{n+3}...I_N I_1 I_2...I_{n1}+ (i_{n+2}1)I_{n+3}I_{n+4}...I_N I_1 I_2...I_{n1} + ... + (i_N 1)I_1 I_2...I_{n1} + (i_1 1)I_2 I_3...I_{n1} + (i_2 1)I_3 I_4...I_{n1} + ... + i_{n1}$.

The introduced SVD can be applied to the matrix unfolding and this is the reason for considering these matrices here for the rank reduction when the HOSVD is adopted. It is possible to demonstrate that the unfolding matrix related to the nth dimension of the tensor (i.e. to the nth mode) can be decomposed as:

$$\mathbf{A_n} = \mathbf{U^n \Sigma^n V^{n^T}} \qquad (6)$$

where $\mathbf{U^n}$ is already introduced decomposing the tensor $\mathcal{A}$ and its columns are the n-mode singular vectors, $\mathbf{\Sigma^n}$ is a diagonal matrix (exactly as in the SVD) and the n-mode singular values of $\mathcal{A}$, $(\sigma_1^n, \sigma_2^n, ..., \sigma_{I_n}^n)$, are on the diagonal.

Using the HOSVD the rank reduction must be just in the dimension related to the parameter variations in order to have high accuracy in the description and uncertainty quantification of the correlated IQs. Thus, using the HOSVD, the matrix unfolding $\mathbf{A_1}$ is considered, since 1 is the dimension of the defined data tensor related to the parameter variations, and the reduction is just in the 1-mode set of singular vectors $\mathbf{U^1}$. For the reduction, the Captured Energy criterion has been adopted [7]. This method consists of selecting enough singular values of the matrix of interest, $\mathbf{A_1}$ for the considered HOSVD, such that the sum of their squares is a certain percentage T of the total sum of the squared values. The reason for such a decision is that the resulting matrix 'captures' $T\%$ of the Frobenius norm of the full matrix, which is correlated with the energy.

Step 3: Surrogate Modelling Surrogate models are then developed for each column of the reduced matrix $\mathbf{U_k^1}$, modelling how they vary with respect to the design parameters. Figure 8 clarifies how the HOSVD is applied and then the surrogate models developed for the analysed problem; the bending moment and the torque are the IQs and the variation in terms of mass of engine (M) and pylon stiffness (E) are considered. It is recommended to consider different surrogate models and to evaluate the one that performs best using the responses obtained at the validation points.
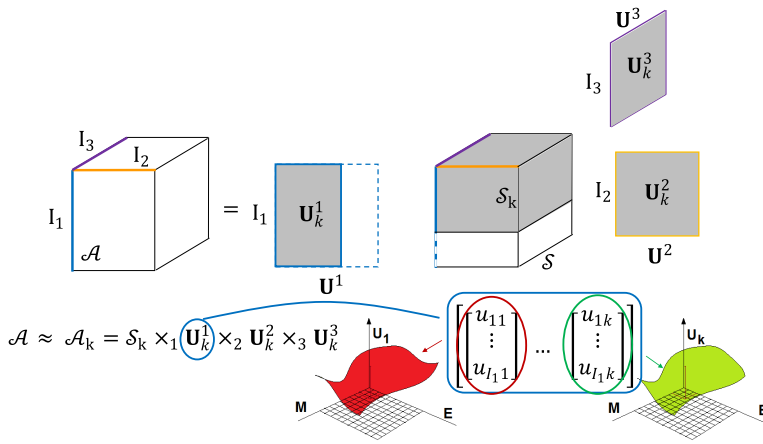
Figure 8: Example of Surrogate Modelling Approach considering the HOSVD as feature extraction.
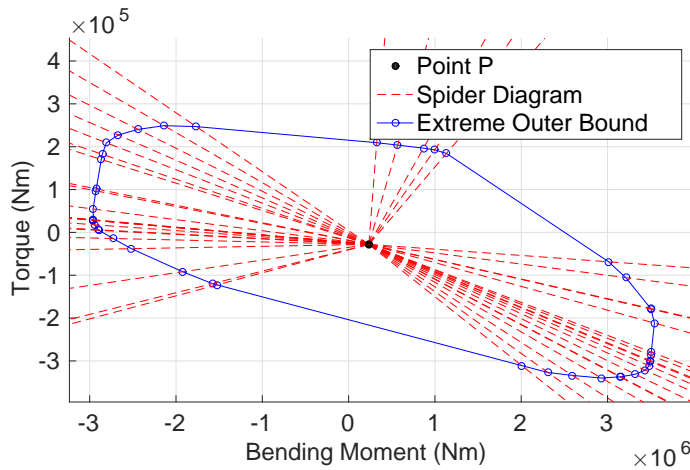

Figure 9: Spider diagram defined at the wing root in order to apply the geometrical based method and detect the probability-bounds.

In the same way as when the SVD is used, the time histories of each IQ at different stations, for different configurations / atmospheric conditions and for a specific i^{th} sampling point can be simply identified by multiplying the respective row vector of coefficient $(\mathbf{U_k^1})_i$, determined by evaluating the surrogate models at the specific i^{th} sampling point in the parameter space, by the basis $\mathcal{S_k} \times_2 \mathbf{U_k^2}... \times_D \mathbf{U_k^D}$ which is assumed not to change throughout the design space.

A major advantage of the developed method is the possibility to completely identify the cases (e.g. gust length), configuration and time instant which give the critical points of any part of the convex hull whatever the decomposition adopted for feature extraction.

Step 4: Detection of angles of interest The Geometrical Based Method developed here is aimed at predicting the effect of uncertainties on the correlated aircraft loads described using the convex hull (or 'potato') plots, whilst still keeping all the information about correlation. In order to completely capture the correlation of loads, a point P_i, $i = 1...S$, and a spider diagram, corresponding to each station, must be defined in the correlated load plot as shown in Figure 9.

Using the SVD/HOSVD based method both the point P_i and the spider diagram can be identified. The point P_i has to be selected such that it is inside all the 'potato' plots obtained at a particular station for the sampling points considered to perform the Uncertainty Quantification; the time-responses are determined using the SVD/HOSVD based method without running the numerical model and saving time. The spider diagram is described by the set of angles α_i, $i = 1...S$, needed to capture the
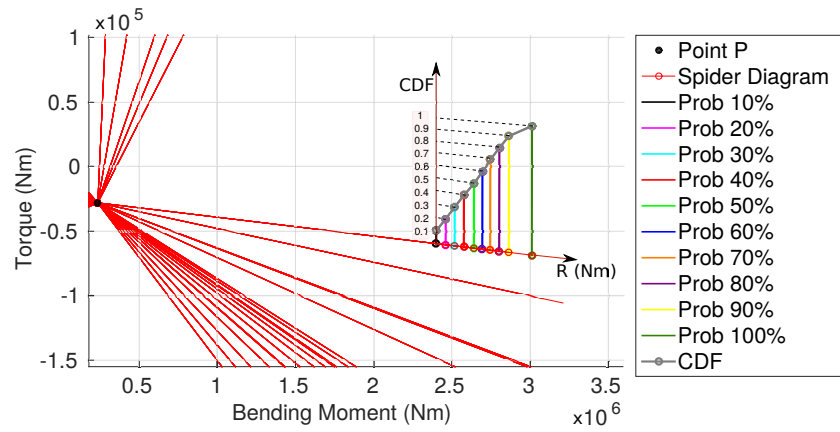
Figure 10: Probabilistic description of radii to determine the bounds for each desired quantile.

critical correlated loads at each station. The set of angles can be selected exploiting the results obtained and presented in [19]. The significant directions are assumed to be captured by the extreme worst case scenario for the correlated loads, which is detected using the interval approach [19]. Further directions can be considered, for example using the results obtained with the quantile-approach [19]. The angles α_i can be defined as those formed by the x-axis and the segment that starts at the defined point P_i and ends at the critical vertices of the determined extreme worst outer bound. The point P and the spider diagram shown in red in Figure 9 are obtained at the wing root following such an approach.

Step 5: Probabilistic-bounds of convex hull An arbitrary high number N of sampling points across the entire parameter space can be considered to evaluate IQs using the SVD/HOSVD based method. Then, at each station statistical quantities (PDF and CDF) can be detected for the radii of the convex hull that start at the defined point P_i and end at the critical vertices related to the angles α_i. For the sake of clarity Figure 10 presents how the CDF of the radii is determined in a particular direction of the spider diagram at the wing root. Different colours are considered for different values of the CDF.

The last step to fully describe the critical cases is to find the correlated loads belonging to the responses evaluated using the SVD/HOSVD based method and nearest to the probabilistic bounds determined using the geometrical based method. In fact, the probabilistic bounds and relative critical vertices, described so far, are obtained as intersections of the spider diagrams with the lines defining the convex hulls obtained at the selected high number N of sampling points. Thus, the points defining the geometrical probabilistic bounds are not guaranteed to belong to any time history.

The next step presents how to fulfill the stated identification.

Step 6: Critical cases detection

The geometric information needs to be related to the correlated loads generated using the SVD/HOSVD based method.

First, the angular direction (clockwise or counter-clockwise) to be considered must be decided and a minimum and maximum absolute radial distance d_R from the segments whose endpoints are the geometrical critical vertices of the probability-bounds. Then, for each of the geometrical probability-bounds, the critical cases in the correlated loads plot are looked for in an iterative process starting from a segment whose endpoints are two consecutive geometrical critical vertices. For the considered segment, the points belonging to one of the N evaluated time-responses are
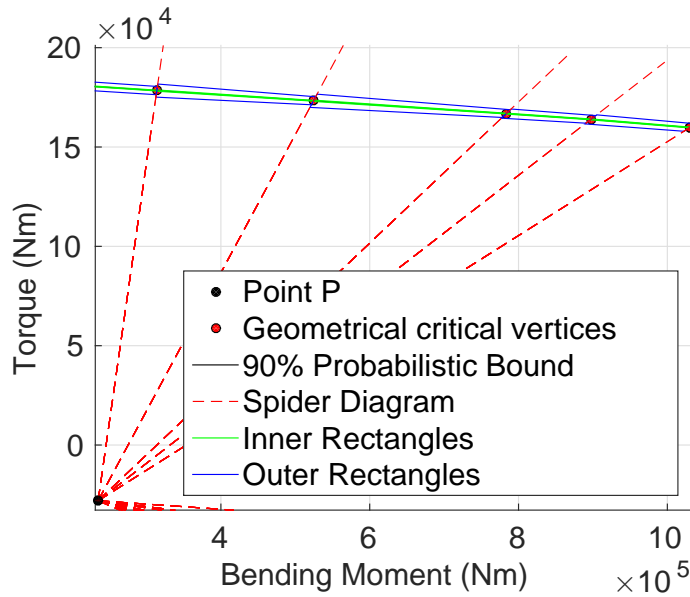
Figure 11: Extreme inner and outer rectangles used to detect the correlated load values belonging to the responses evaluated using the SVD/HOSVD based method and nearest to the 90% probabilistic bounds determined using the geometrical based method.
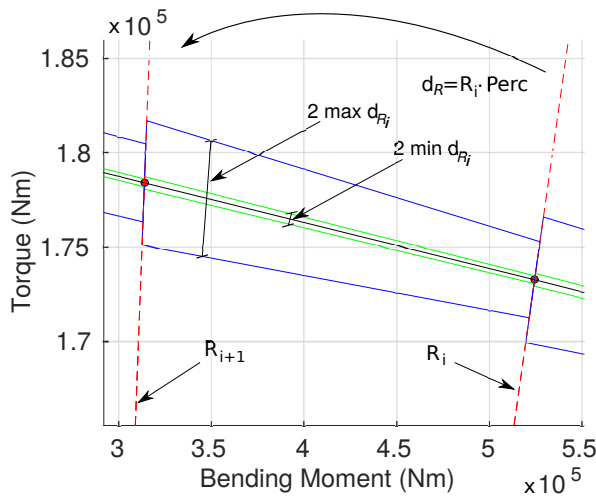

Figure 12: Zoom of Figure 11 to show one of the particular set of the adopted extreme inner and outer rectangles.

looked for in a particular rectangle. The vertices of this rectangle are firstly set at plus and minus the minimum d_R in the radial direction from the two endpoints of the considered segment and towards the point P_i. d_R is iteratively increased if no points are found. If, eventually, the maximum value of d_R is reached, then, the second endpoint of the segment is set to the the following critical vertex, according to the decided angular direction. Figures 11 and 12 show how the stated rectangles are constructed. In particular, the rectangles shown in Figure 11 and 12 are those related to the minimum and maximum values selected for d_R ($mind_R$, $maxd_R$) which are here defined as a percentage ($Perc$) of R_i, which is the length of the radius connecting the point P with the geometrical critical vertex i. Here, $mind_R$ and $maxd_R$ are fixed equal to $0.001 \cdot R_i$ and $0.01 \cdot R_i$, respectively.

Figure 13 shows an example of the results that can be obtained after having applied the geometrical based method and used the rectangles to identify the critical vertices that belong to one of the N evaluated time-responses (obtained using the SVD/HOSVD method), which are represented with blue dots in the picture. The red lines define all the considered rectangles around the convex hull. For the sake of clarity, Figure 14 magnifies part of Figure 13 to better show how the stated critical vertices can be identified

Figure 13: Results obtained after having applied the geometrical based method to identify the 90% probabilistic bound. The 'rectangle-technique' has then been used to identify the critical vertices that belong to one of the N evaluated time-responses (obtained using the SVD/HOSVD method), which are represented with blue dots in the picture. The red lines define all the considered rectangles around the convex hull.
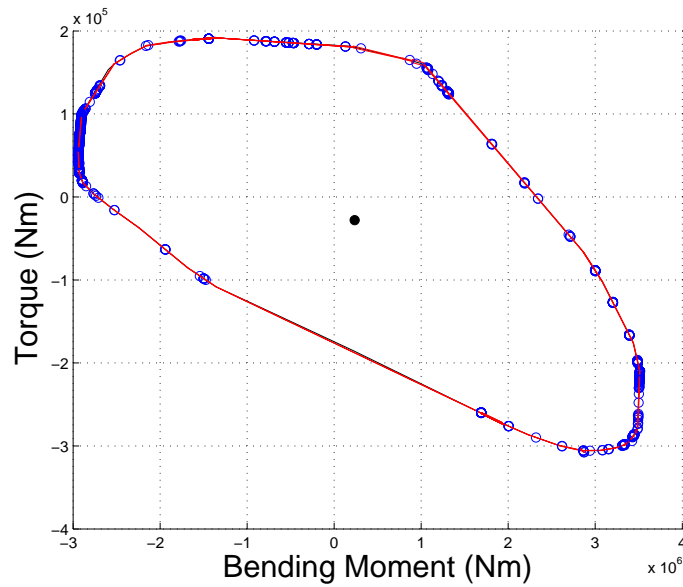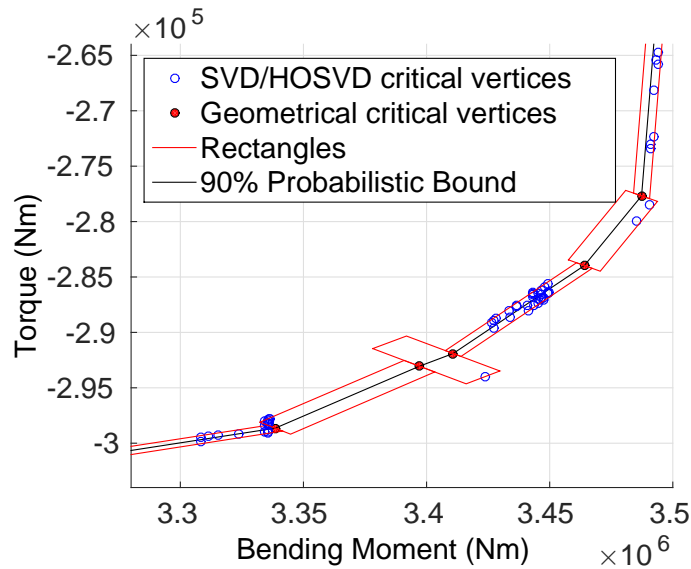

Figure 14: Magnification of Figure 13 to show in detail how the rectangles are defined in order to detect the critical vertices related to correlated quantities obtained with the SVD/HOSVD based method.

adopting the 'rectangles-technique'; the geometrical critical vertices are represented as red dots.

A final step that could be useful in the presence of an excessive number of critical vertices, obtained applying the geometrical based method and the 'rectangle-technique' procedure, is to apply the convex hull to the detected points. In such a way a reduction of critical cases is achieved. Figure 15 is the result obtained applying the convex hull to the points shown in Figure 13.

4.1 Accuracy Discussion

The accuracy of the results given by the Uncertainty Quantification can be discussed using a particular 'radial error metric' based on the spider diagram description. The spider diagram is defined for each station and by the angles $\alpha_{\mathbf{cr_i}}$, which are formed by the x-axis and the radius that starts at the defined point P_i and ends at the critical vertices, on the analysed probabilistic-bound, whose coordinates are correlated quantities belonging to one of the N evaluated time-responses (obtained using the SVD/HOSVD method). The difference with
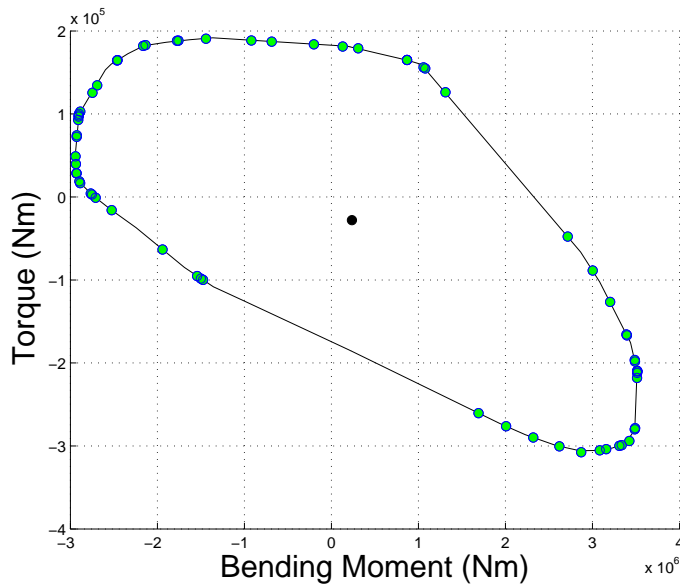
Figure 15: Reduction of critical vertices shown as blue dots in Figure 13 obtained simply applying the convex hull to the whole set of points.
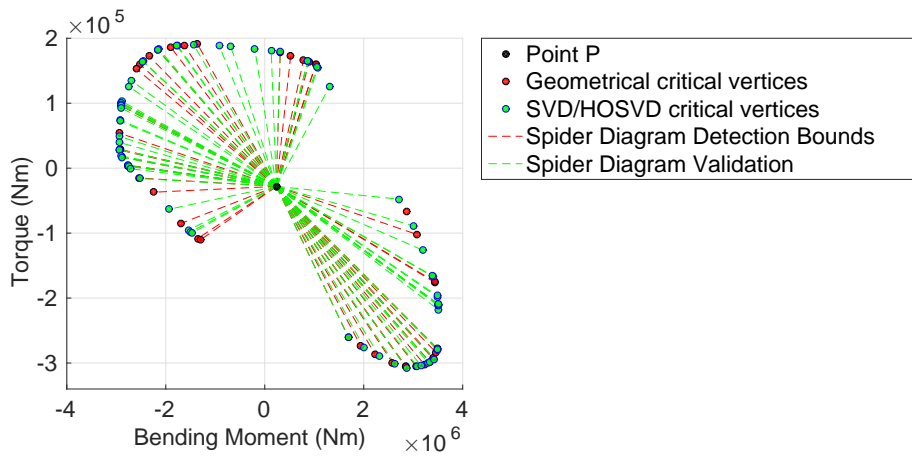

Figure 16: Comparison of the spider diagrams defined to perform UQ and their validation.

the spider diagram adopted for the UQ is in the critical vertices adopted to define the set of angles $\alpha_{\mathbf{cr_i}}$, as shown in Figure 16.

The 'radial error metric' can be defined using the convex hull (and time-responses) obtained for the last set of validation points (see first step of the geometrical based method) at each station. For each station, the Mean Average Percentage Error (MAPE) of the distance between the point P_i and the intersection between the 'actual'/SVD or HOSVD convex hulls and the semi-straight line that starts at P_i and has direction $\alpha_{\mathbf{cr_i}}$, is considered. Mathematically, this can be expressed as

$$MAPE = \frac{1}{D_{i,q}} \sum_{j=1}^{D_{i,q}} \left| \frac{\hat{R}_j - R_j}{R_j} \right| \quad i = 1...S \qquad q = 1...Q \tag{7}$$

where $D_{i,q}$ is the dimension of $\alpha_{\mathbf{cr_i}}$ at the station i and for a probability fixed equal to q, S is the total number of stations, Q is the number of considered probability, R_i and $\hat{R}_i$ are the radii obtained using the validation points and the result of the geometrical based method.

For the sake of clarity, Figure 17 shows an example of two convex hulls obtained at a validation point, using directly the numerical model ('Actual' convex hull) and the HOSVD based method, and the directions considered to evaluate the 'radial error metric' as just stated. Figure 18 magnifies part of Figure 16 and x marks are used to underline the intersections identifying the

Figure 17: Spider diagram adopted for the validation and comparison of an 'actual' convex hulls and one obtained using the HOSVD method and the geometrical based method at some validation points.
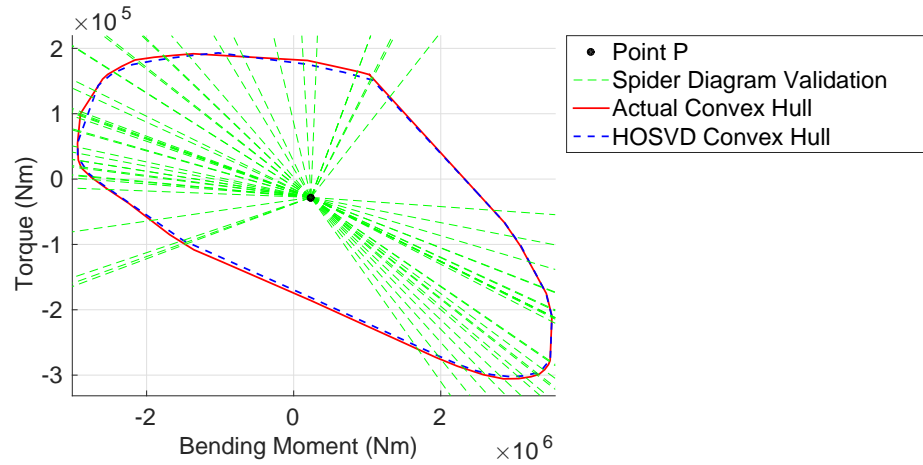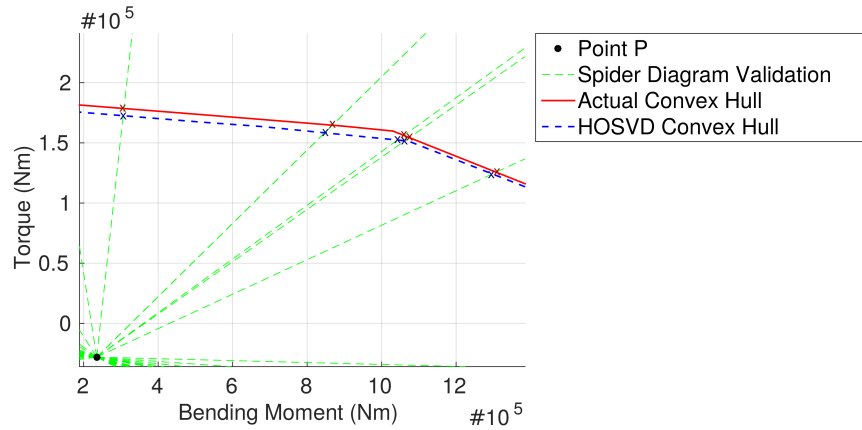

Figure 18: Magnification of part of Figure 17. The x mark has been used here to underline the intersections that define the radius R_i and $\hat{R}_i$ adopted in the the 'radial error metric'

sought length of interest R_i and $\hat{R}_i$.

5   Results and discussion

In this section the results of the developed geometrical based method applied to data from the simulated civil aircraft model are presented. The discussion is divided into two parts: the first one covers the steps related to the data generation, application of the SVD/HOSVD approach and surrogate models; the second presents results obtained using the geometrical based method.

5.1   Data generation, SVD/HOSVD and Surrogate Models

The Latin Hypercube Sampling method [16], was used to define the sampling points for training, validation and best surrogate model selection due to its characteristic in providing unbiased estimates for statistical variables and not overlapping sampling points that can cover a large range without using a lot of points. Sampling planes of 100, 30 and 1200 points respectively were used for the training, validation of the surrogate models and the discussion of the accuracy reached with the geometrical based method to propagate the uncertainty.

Once the data is generated, the data matrices/tensor have been constructed and reduced using the Captured Energy criterion and fixing T equal to 99.9999 (see section 4 for further details). The HOSVD required 29 surrogate models while the SVD required 27+37 models for the bending moment and torque matrices, respectively. Just for the SVD, since it was already adopted in previous work, [19] without applying the Energy criterion but looking at the variation of the accuracy changing the number of singular values to be retained, the stated criterion has not been considered. The same reduction done in [19] using the
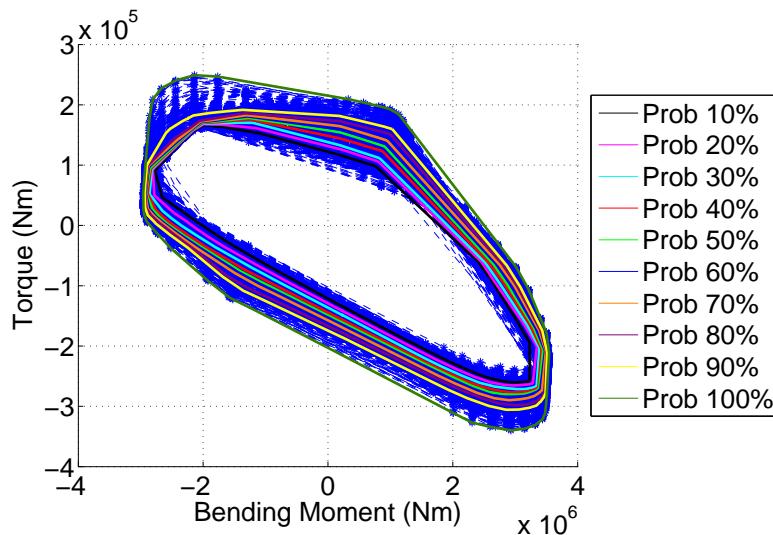
Figure 19: Convex hull obtained exploiting the HOSVD based method for fixed desired probabilities.

SVD has been adopted, namely 1 and 30 surrogate models for the bending moment and torque matrices.

The Blind Kriging Surrogate has been adopted both for the SVD and HOSVD based methods as its accuracy for such an application has already been demonstrated [19]. Both the validation of the surrogate models trained for the SVD and the HOSVD based method show the same level of accuracy, with a MAPE always less than 1% for the bending moment and 8% for the torque.

5.2 Geometrical based method

The angles α_i needed to define the spider diagram (section 4, step 4) have been selected as those characterizing the outer bounds obtained using the interval and quantile approaches described in [19]. Using this spider diagram, the probabilistic-bounds were determined using the approach explained in section 4 step 5. It is worth emphasizing that the number of considered varying parameters does not directly influence a change in the convex hull; rather, it is the particular parameter that is varied that can affect the extent to which the shape of the convex hull changes. However, thanks to the adopted geometrical based method, the determined spider diagram is all that is needed to capture the behaviour of the IQs given the range of the uncertain parameters.
Figure 19 shows the probabilistic-bounds obtained considering 1200 convex hulls that were created using the HOSVD based method. The use of ether the HOSVD or SVD based method speeds up the analysis because the surrogate models are used to obtain the time-responses instead of running the numerical model. Moreover, in the present application the HOSVD required a lower number of surrogate models to be trained if compared to the SVD method, but keeping the same accuracy; thus a further speeding up of the analysis has been achieved. The reduction using the ROM method is about 100% compared to the monte-carlo approach. A similar difference in computation time was observed in tests where five uncertain parameters were considered. [19].

After having obtained the probabilistic-bounds, this information can be mapped onto the correlated loads plots using the approach described in section 4, step 6.

Figure 20 shows a comparison of the actual 90% probabilistic-bounds with the one obtained using the SVD and HOSVD based methods at the wing root. The actual bounds are determined using the time-histories related to the last validation sampling plane (section 4, step 1). The 'radial error metric', described in subsection 4.1, has been considered to assess the accuracy of the performed Uncertainty Quantification and the results are very encouraging. For the sake of
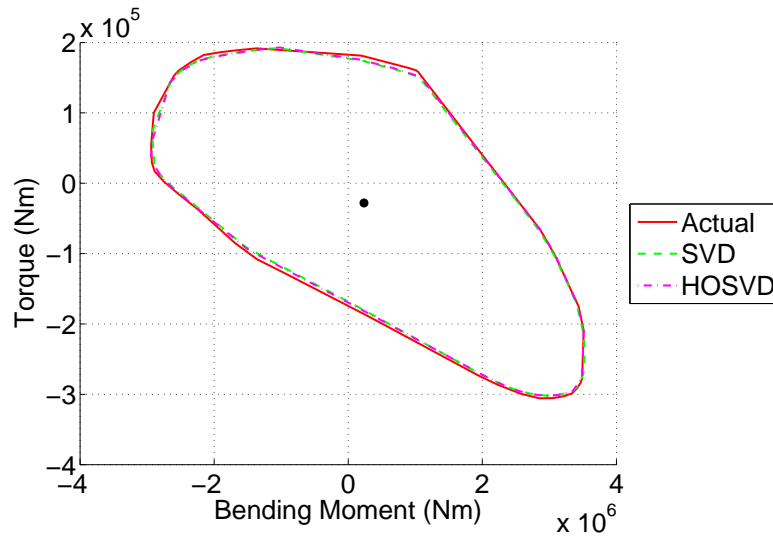
Figure 20: Comparison of the actual convex hull with those obtained having fixed the desired probability to 90% and using the SVD and the HOSVD based methods.

Table 2: MAPE obtained comparing the actual convex hull and those obtained applying the SVD/HOSVD based method for different selected probability.

Probability (%)	MAPE	
	SVD (%)	HOSVD (%)
10	3.24	2.68
20	2.17	1.82
30	1.47	1.22
40	1.75	1.32
50	1.38	1.12
60	1.23	0.97
70	1.20	0.96
80	1.44	1.22
90	1.29	1.14
100	1.28	1.31

completeness, Table 2 shows the MAPE calculated for 10 different probabilities, always for the wing root, and the high accuracy is apparent.

Finally, Figure 21 and Table 3 are presented in order to show that the developed method enables information about the critical cases to be retained. Figure 21 shows the critical vertices on the correlated loads plots and for different gust lengths. Table 3 provides information about design parameters (mass of engine and pylon Young Modulus) and load cases (gust lengths) related to some of the critical cases shown in Figure 21.

With respect to the correlation between the different stations along the wing, Figures 22 and 23 shows the values of the IQs (bending moment and torque) at different stations and at the critical cases obtained for the loads at the wing root.

The geometrical based method gives the exact uncertainty bounds of the

Table 3: load cases (gust lengths L_g) and values of design parameters (mass of engine m_e and pylon Young modulus E) at some of the critical cases shown in Figure 21 identified using the geometrical based method and using the HOSVD.

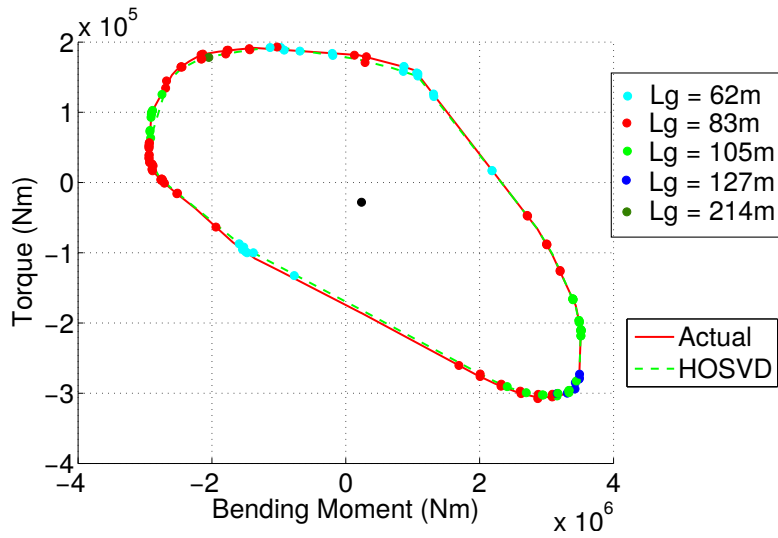| Angle	$L_g(m)$	$m_E(kg)$	$E(Pa)$
1.31	62	8133.78	7.44E+10
7.92	62	8503.93	6.15E+10
12.05	62	8314.93	7.02E+10
154.04	62	8666.23	7.17E+10
172.59	83	8800.87	6.55E+10
174.83	214	8643.28	6.48E+10
178.34	105	8478.61	6.89E+10
185.94	62	9109.39	7.34E+10
353.12	105	8490.47	6.36E+10
354.68	127	8831.00	7.48E+10

Figure 21: Critical cases for the 90% probabilistic-bounds of the convex hull at wing root. Suitable rectangles are considered in order to identify such critical cases (section 4).
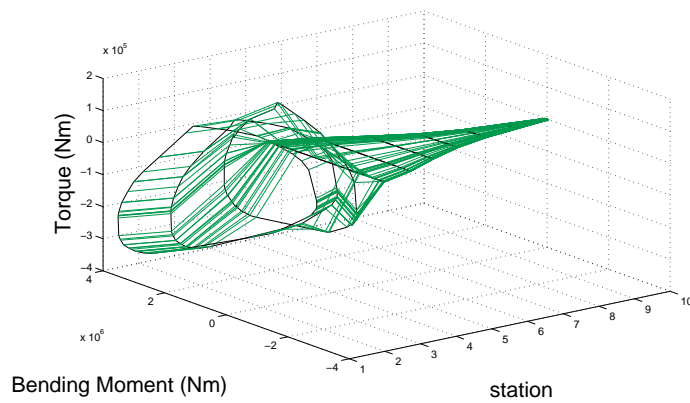

Figure 22: Loads along the span of the wing correlated to the critical cases determined for the wing root.
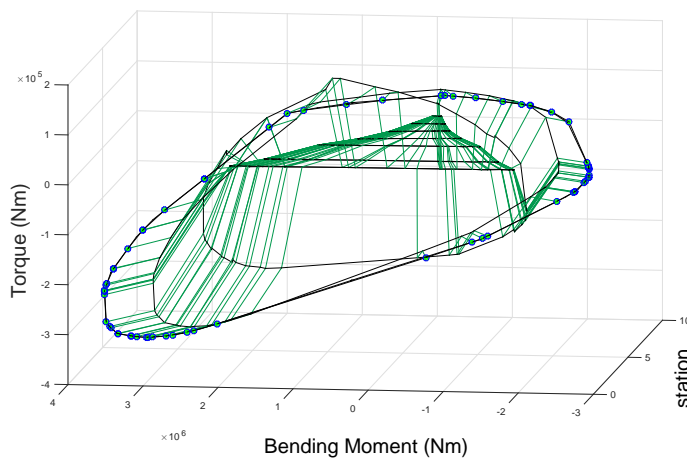

Figure 23: Different point of view of Figure 22.

convex hull for any level of desired probability. The critical points on the convex hull can be obtained using the mapping procedure described in section 4. The method is 160% more time consuming than the approach exploiting the use of quantiles in terms of 'time-histories' [19]. However, it maintains the correlation of loads during the uncertainty management and there are no assumptions that can influence the obtained outer bounds as happens if the quantile approach is applied (see section 2).

6   Conclusions

A geometrically based method has been developed to efficiently predict the probabilistic bounds of correlated aircraft loads and to relate the critical cases back to the corresponding configuration, flight conditions and load cases. The strength of the developed method is also in the inherent generalization of the kind of input loads among which the critical loads can be searched. The case study has shown that it is possible to accurately determine the geometrical probabilistic bounds on correlated loads plots due to variations in the aircraft structural parameters. The accuracy has been critically discussed, defining a suitable 'radial error metric'. The method is shown to address the possible inaccuracies that could occur with a previous time history quantile bound method. Both SVD and higher order SVD approaches have been used to identify the underlying reduced order model and it has been found that the HOSVD approach requires a substantially reduced order surrogate model if the Energy Criterion is considered. The methodology developed in this paper has the potential to significantly reduce the amount of computational resources required to not only determine the worst case 1D and correlated loads for airworthiness certification, but also to quantify the effects of uncertainty on the process. The approach is totally general and could be extended to include all types of loads that have to be considered eg. manoeuvres and ground loads.

7   Acknowledgements

References

[1] K.J. Badcock, H.H. Khodaparast, S. Timme, and J.E. Mottershead. Calculating the influence of structural uncertainty on aeroelastic limit cycle response. *52nd AIAA/ASME/ASCE/AHS/ASC Structures, Structural Dynamics, and Materials Conference*, April 4-8 2011. Denver, Colorado.

[2] S. K. Choi, R. V. Grandi, and R. A. Canfield. *Reliability-based Structural Design*. Springer-Verlag London Limited, 2010.

[3] M. S. Eldred. Recent advances in nn-intrusive polynomial chaos and stochastic collocation methods for uncertainty analysis and design. *50th AIAA/ASME/ASCE/AHS/ASC Structures, Structural Dynamics, and MAterla COnference*, 4-7 May 2009. Palm Springs, California.

[4] G. Georgiou, A. Manan, and J.E. Cooper. Modeling composite wing aeroelastic behaviour with uncertain damage severity and material properties. *Mechanical Systems and Signal Processing*, 32:pp. 32–43, October 2012.

[5] F. M. Hoblit. *Gust Loads on Aircraft Concepts and Applications*. AIAA, 1988.

[6] M. Ishteva, P. A. Absil, S. Van Huffel, and L. De Lathauwer. Best low multilinear rank approximation of higher-order tensors, based on the Riemannian trust-region scheme. *SIAM J.Matrix Anal. Appl.*, 32(1):pp 115–135, 2011.

[7] Emiliano Iuliano and Domenico Quagliarella. Evolutionary optimization of benchmark aerodynamic cases using physics-based surrogate models. *53rd AIAA Aerospace Science Meeting*, January 5-9 2015. Kissimmee, Florida USA.

[8] H. H. Khodaparast and J. E. Cooper. Rapid prediction of worst case gust loads following structural modification. *AIAA Journal*, 52(2):242–254, 2014.

[9] H. H. Khodaparast, J. E. Cooper, L. Cavagna, S. Ricci, and L. Riccobene. Fast prediction of worst case gust loads. *International Forum on Aeroelasticity and Structural Dynamics*, 2013.

[10] H. H. Khodaparast, G. Georgiou, J. E. Cooper, L. Travaglini, S. Ricci, P. Denner, and G. A. Vio. Efficient worst case '1 cosine' gust loads prediction. *IFASD 2011 Paris*. Paris, France.

[11] H. H. Khodaparast, G. Georgiou, J. E. Cooper, L. Travaglini, S. Ricci, G. A. Vio, and P. Denner. Rapid prediction of worst case gust loads. *Journal of Aeroelasticity and Structural Dynamics*, 2(3), 2012.

[12] L. De Lathauwer, B. De Moor, and J. Vandewalle. A multilinear singular value decomposition. *SIAM J.Matrix Anal. Appl.*, 21(4):pp 1253–1278, 2000.

[13] T. L. Lomax. *Structural Loads Analysis for Commercial Transport Aircraft: Theory and Practice*. AIAA Education Series, 1999.

[14] Manan and J.E. Cooper. Design of composite wings including uncertainties - a probabilistic approach. *Journal of Aircraft*, 46(2):pp. 601–607, 2009.

[15] Q. Ouyang, X. Chen, and J. E. Cooper. Robust aeroelastic analysis and optimization of composite wing under -analysis framework. *Journal of Aircraft*, 50:pp. 1299–1305, 2013.

[16] A. Saltelli, K. Chan, and E. M. Scott. *Sensitivity Analysis*. Wiley, first edition, 2009.

[17] C. Scarth, J. E. Cooper, P. M. Weaver, and G. H. C. Silva. Uncertainty quantification of aeroelastic stability of composite plate wings using lamination parameters. *accepted for Composite Structures*. http://dx.doi.org/10.1016/j.compstruct.2014.05.007.

[18] C. Scarth, P. Sartor, J. E. Cooper, P. M. Weaver, and G. H. C. Silva. Robust aeroelastic design of composite plate wings. *17th AIAA Non-Deterministic Approaches Conference*, January 5-9 2015. Orlando, Florida USA.

[19] I. Tartaruga, J. E. Cooper, M. H. Lowenberg, P. Sartor, S. Coggon, and Y. Lemmens. Prediction and uncertainty propagation of correlated time-varying quantities using surrogate models. *CEAS Aeronautical Journal*, 7(1):pp. 29–42, March 2016.

[20] I. Tartaruga, J. E. Cooper, M. H. Lowenberg, P. Sartor, and Y. Lemmens. Evaluation and uncertainty quantification of bifurcation diagram: Landing gear, a case study. *UNCECOMP*, May 25-27 2015. Crete Island Greece.

[21] I. Tartaruga, J. E. Cooper, P. Sartor, M. H. Lowenberg, S. Coggon, and Y. Lemmens. Efficient prediction and uncertainty propagation of correltated loads. *SCITECH2015*, January 5-8 2015. Orlando, Florida USA.

[22] M.T. Tong. A probabilistic approach to aeropropulsion system assessment. *NASA Technical Reports Server NASA/TM-2000-210334*. Glenn Research Center, Cleveland, Ohio, USA.

[23] J. R. Wright and J. E. Cooper. *Introduction to Aircraft Aeroelasticity and Loads*. Wiley, 2007.

[24] D. Xiu and G. E. Karniadakis. The wiener-askey polynomial chaos for stochastic differential equations.